

Radio counterparts of ultraluminous X-ray sources in nearby galaxies

YIJIA ZHANG,¹ HUA FENG,² AILING WANG,² AND ROBERTO SORIA³¹Department of Astronomy, Tsinghua University, Beijing 100084, People's Republic of China²State Key Laboratory of Particle Astrophysics, Institute of High Energy Physics, Chinese Academy of Sciences, Beijing 100049, People's Republic of China³INAF-Osservatorio Astrofisico di Torino, Pino Torinese, Italy

ABSTRACT

Radio surveys of ultraluminous X-ray sources (ULXs) allow us to find supercritically accreting compact objects (SS 433/W50 like systems) or stripped nuclear black holes in nearby galaxies. We identified 21 such objects by crossmatching a ULX catalog with the Rapid ASKAP Continuum Survey (RACS) and Very Large Array Sky Survey (VLASS). They may have a diverse population. (i) Three have a double lobed radio structure with a compact core found in two of them, and could be quasars. (ii) Five are associated with extended radio structure and star forming regions in optical, where the radio emission is likely due to star forming activities, although the steep radio spectrum up to several GHz casts doubt on that. Two of them show X-ray variability suggesting that they are ULXs embedded in star forming regions. (iii) Thirteen are associated with an unresolved radio source, with a steep spectrum seen in eight, a flat or inverted spectrum seen in two. Those with a steep spectrum are arguably candidates for SS 433/W50 like objects, with radio emission due to optically thin synchrotron radiation in a surrounding jet/wind powered nebula. Remarkable cases include NGC 925 ULX1 and NGC 6946 ULX1, which are associated with an optical nebula. Those with a flat or inverted spectrum could be accreting black holes with a compact jet, while the black hole mass is estimated to be several $10^6 - 10^8 M_{\odot}$ based on the fundamental plane. Redshift measurements are needed to firmly determine the association with their apparent host galaxy.

1. INTRODUCTION

Ultraluminous X-ray sources (ULXs; Kaaret et al. 2017; Fabrika et al. 2021; King et al. 2023) are non-nuclear X-ray sources with an isotropic luminosity exceeding 10^{39} erg s⁻¹ or the Eddington limit of a stellar mass black hole. The nature of ULXs is still unclear, and they may contain a diverse population (Feng & Kaaret 2005; Earnshaw et al. 2019; Tranin et al. 2024).

The majority of ULXs are believed to be powered by supercritical accretion onto stellar mass compact objects, as evidenced by the identification of pulsars in ULXs (e.g. Bachetti et al. 2014). In the regime of supercritical accretion, radiation pressure will be dominant in the accretion flow and drive massive winds (Meier 1982; Poutanen et al. 2007; Ohsuga & Mineshige 2011; Jiang et al. 2014; Sadowski & Narayan 2016; Kitaki et al. 2021). X-ray spectroscopy has revealed blueshifted absorption features in the spectrum of ULXs (Walton et al. 2016; Pinto et al. 2016, 2017, 2021; Kosec et al. 2018), suggesting that relativistic winds are indeed present in them (for a review see Pinto & Walton 2023). These outflows will eventually interact with the ambient medium and produce shock-ionized nebulae, seen as optical emission line bubbles surrounding the ULXs (Pakull

& Mirioni 2002, 2003; Ramsey et al. 2006; Abolmasov et al. 2007; Abolmasov 2008; Russell et al. 2011; Soria et al. 2021; Gúrpide et al. 2022; Zhou et al. 2022, 2023a,b).

Alternatively, a small fraction of ULXs may contain intermediate mass black holes (IMBHs) with a mass in the range of $10^2 - 10^5 M_{\odot}$ (Colbert & Mushotzky 1999). In particular, the search of IMBHs focuses on ULXs at the high luminosity end (Sutton et al. 2012; Barrows et al. 2019; MacKenzie et al. 2023), known as hyper-luminous X-ray sources (HLXs) with a luminosity in excess of 10^{41} erg s⁻¹ (Gao et al. 2003; Amato et al. 2025). Remarkable candidates for IMBHs include ESO 243-49 HLX-1 (Farrell et al. 2009; Servillat et al. 2011) and M82 X-1 (Feng & Kaaret 2010; Pasham et al. 2014).

In general, supermassive black holes are not expected at nonnuclear positions due to dynamical friction (Tremaine et al. 1975). However, they may reside in ultracompact dwarf galaxies as a result of tidal stripping during galaxy merger, with a black hole mass in the range from IMBH up to $10^8 M_{\odot}$ (Seth et al. 2014; Graham et al. 2025). If they undergo active accretion, they may appear as ULXs. However, no such cases have been observed.

Radio observations of ULXs have produced useful constraints on their nature. In most cases, the radio emission is found to be optically thin and extended, spatially coincident with the optical nebula, suggesting that the emission is also produced by shocks due to wind/jet interaction with the interstellar medium (van Dyk et al. 1994; Lacey et al. 1997; Miller et al. 2005; Lang et al. 2007; Cseh et al. 2012; Urquhart et al.

Corresponding author: Hua Feng
hfeng@ihep.ac.cn

2018; Berghea et al. 2020; Soria et al. 2021). In a few cases, a compact radio core is detected with the very long baseline interferometry (VLBI), allowing for black hole mass estimation assuming jet emission in the fundamental plane (Mezcua & Lobanov 2011; Mezcua et al. 2013). If this assumption is valid, their typical X-ray and radio luminosities would generally suggest the presence of IMBHs (cf., Table 3 in Mezcua et al. 2013). Transient radio emission was detected in HLX-1, offering us the opportunity to constrain the black hole mass to be $< 2.8 \times 10^6 M_\odot$ assuming the source was observed in the fundamental plane and considering that the radio emission might have been Doppler boosted (Webb et al. 2012; Cseh et al. 2015).

SS 433, a microquasar in the Milky Way, has long been considered analogous to ULXs, as it is thought to be powered by supercritical accretion from an evolved massive star onto a black hole candidate (for a review see Fabrika 2004). However, the X-ray emission from the compact object is rather faint; it is speculated that thick outflows may have obscured the intrinsic X-ray emission (Fabrika et al. 2021). SS 433 itself is a bright radio source (~ 1 Jy) due to a pair of precessing, relativistic jets, which drive a radio nebula W50 (71 Jy at 1.4 GHz with an extent of about 2°) further out when interacting with the surrounding medium (Dubner et al. 1998). NGC 7793 S26 is one of the best extragalactic analogs to SS 433 and shows a pair of lobes with emission in X-ray, optical emission line, and radio (Pannuti et al. 2002; Pakull et al. 2010; Soria et al. 2010b), driven by shocks with a total mechanical power of about 10^{40} erg s $^{-1}$. Other similar cases include NGC 300 S10 (McLeod et al. 2019; Urquhart et al. 2019) and M83 MQ1 (Soria et al. 2014) and S2 (Soria et al. 2020). If SS 433/W50 were located in a nearby galaxy at a distance that is 10^3 times greater, and we observed the system along its symmetric axis, we would observe a ULX associated with a radio nebula.

Thus, radio observations provide a distinctive means to explore the physics of supercritical accretion or to identify IMBHs. Previously, radio emission in ULXs have been systematically searched with the Faint Images of the Radio Sky (FIRST) survey (Sánchez-Sutil et al. 2006; Pérez-Ramírez et al. 2010), resulting in useful candidates for in-depth case studies. The FIRST survey was conducted with VLA at 20 cm with a root-mean-square (rms) of 0.15 mJy and an angular resolution of $5''$. Today, radio surveys with a better sensitivity and angular resolution are available, including the Rapid ASKAP Continuum Survey (RACS; McConnell et al. 2020) and the Very Large Array Sky Survey (VLASS; Lacy et al. 2020). Therefore, in this work, we aim to perform a new search of radio emission in ULXs using these radio archives (§ 2). Follow-up observations of some of the selected objects with the Australia Telescope Compact Array (ATCA) were conducted (§ 2.1). The detailed results for each object in the crossmatched sample are shown in § 3. We discuss their possible physical nature in § 4 with a summary in § 5.

2. SAMPLE, OBSERVATIONS, AND ANALYSIS

We adopted the ULX catalog of Walton et al. (2022), which is a compilation of the Chandra Source Catalog Release 2 (CXC2; Evans et al. 2024), the fourth XMM-Newton serendipitous source catalog (4XMM; Webb et al. 2020), and the second Swift X-ray Point Source catalog (2SXPS; Evans et al. 2020), containing 1843 ULXs in nearby galaxies. The RACS and VLASS radio surveys are used for searching for their radio counterparts. Two bands of RACS are used, the RACS-low at 0.9 GHz with a bandwidth of 288 MHz and RACS-mid at 1.4 GHz with a bandwidth of 144 MHz. The central frequency of VLASS is 3 GHz and the bandwidth is 2 GHz. The spatial resolution is in the range of $15''$ – $25''$ for RACS-low and $\gtrsim 8''$ for RACS-mid, and the sensitivity is 0.2–0.4 mJy beam $^{-1}$ and 0.15–0.4 mJy beam $^{-1}$ for the two bands, respectively (Duchesne et al. 2023). For VLASS, the beam size is about $2''/5$ and the 5σ sensitivity is around 0.35 mJy beam $^{-1}$ (Lacy et al. 2020). The RACS survey mainly covers the southern sky ($\delta < +40^\circ$) and VLASS mainly covers the northern sky ($\delta > -40^\circ$). The combination of the two surveys allows for a full sky coverage at a similar sensitivity of several hundred μ Jy beam $^{-1}$.

As the radio counterparts could be rather extended, e.g., a double lobed structure, the search is not based on cross-correlation between the source positions. We also realized that some point-like radio sources are not listed in the VLASS source catalog (Gordon et al. 2021) and examination of the image is needed. Thus, we extracted radio images with a dimension of $2' \times 2'$ around the ULX position, and try to identify excessive radio emission that is 4 times above the rms noise. For an unresolved radio source, the 1σ position error is typically the beam size divided by the signal-to-noise ratio, which is used as a rough estimate. In sum, we labeled three types of potential counterparts: (i) the radio peak and X-ray position is consistent within the quadratic sum of their 3σ position errors; (ii) the X-ray position is associated with an extended radio structure; (iii) the X-ray position is along the center of a double lobed structure no matter if there is a radio core around the X-ray position. We selected 21 candidate radio counterparts of ULXs with the above means. Among them, five are associated with extended radio emission, determined if the integrated flux density deviates from the peak flux density by a factor of 2 or more¹, and three are associated with a double lobed structure with two showing a radio core.

We retrieved optical images around the ULX position from the following archives, prioritized by data quality and availability: the Panoramic Survey Telescope and Rapid Response System (PanSTARRS; Chambers et al. 2016), Dark Energy Survey Data Release 2 (DES-DR2; Abbott et al. 2021), and Digitized Sky Survey (DSS). We note that, limited by the sensitivity and resolution of these ground-based optical sur-

¹ We tested the criterion against a sample of compact radio sources (Petrov & Kovalev 2025) with a successful rate of 98% for RACS and 92% for VLASS. We also had visual inspections to see whether the sources are resolved or not. We note that these are all empirical and preliminary.

veyes, the optical counterparts are usually not due to emission from the ULX binary system (Tao et al. 2011) and too bright to be a single star, but could be their host star clusters or host dwarf galaxies, or instead are active galactic nuclei (AGNs) that are masqueraded as ULXs. If no optical counterpart can be seen, an upper limit is estimated based on the nearby, faintest objects. We note that the optical emission is extended for three sources, NGC 2207 ULX3, NGC 2903 ULX3, and NGC 5457 ULX4, and the optical magnitude represents emission from the bright knot associated with the ULX in the star forming region.

We argue that the astrometric uncertainty does not affect counterpart identification. For the Chandra and XMM catalogs, the systematics have been corrected with residuals included in the quoted uncertainties (Evans et al. 2024; Webb et al. 2020). For Swift, the statistical errors dominates (Evans et al. 2020). The optical images have been astrometrically calibrated to a much higher accuracy than in other bands (Abbott et al. 2021; Magnier et al. 2020). The RACS images may have an astrometric uncertainty of around $2''$, much smaller than the source position uncertainty in our cases (Duchesne et al. 2024). For VLASS, the absolute astrometry has an accuracy better than $0''.5$, negligible again (Gordon et al. 2021). Therefore, we conclude that the absolute astrometry is either already corrected or accurate enough compared with statistical uncertainties.

General information of the candidates is listed in Table 1, including the X-ray position and luminosity, distance to the host galaxy, and magnitude of the optical counterpart, etc. The radio contours are plotted on top of the optical images in Figure 1, overlaid with the ULX position error circle. The peak flux densities that are directly measured from the survey images are listed in Table 2, along with the spectral index α ($S_\nu \propto \nu^\alpha$) determined using all available bands.

2.1. ATCA observations

We conducted radio observations (code: C3663) of eight sources (ESO 352-41 ULX1, NGC 1332 ULX2, PGC 146838 ULX1, NGC 2207 ULX3, ESO 171-5 ULX1, NGC 5018 ULX6, ESO 514-3 ULX1, and NGC 7059 ULX1) in our sample with ATCA at 5.5 GHz and 9 GHz to obtain radio images for a better sensitivity and at higher frequencies. The array comprises six 22 m antennas with a maximum baseline of 6 km. Observations in the 4 cm band were carried out at two central frequencies — 5.5 GHz and 9 GHz — each with a 2 GHz bandwidth, using B1934-638 as the amplitude and band-pass calibrator. The data were processed with the Common Astronomy Software Applications (McMullin et al. 2007), including flagging of bad data, calibration, Fourier transformation, deconvolution, and image analysis.

The flux contours are also plotted in Figure 1 along with the survey images. The peak flux density is listed in Table 2. The ATCA observation of each target consists of 2–5 individual observations scheduled in different days. We examined

the flux variation and found two sources with time variability. Their lightcurves are shown in Figure 2.

2.2. X-ray to optical flux ratio

We calculated the X-ray to optical flux ratio following the definition in Maccacaro et al. (1988),

$$\log(f_X/f_V) = \log(f_X) + \frac{m_V}{2.5} + 5.37, \quad (1)$$

where f_X is the observed 0.3–3.5 keV flux, and m_V is the V -band magnitude. The 0.3–3.5 keV flux is transferred from the catalog flux assuming a power-law spectrum subject to interstellar absorption given spectral parameters quoted in the catalog. The V magnitude is translated from the original survey photometry using the recipes in their references (Chambers et al. 2016; Abbott et al. 2021). There are a few cases where the survey does not provide the photometry for the object. We then adopted the Gaia (Gaia Collaboration et al. 2023) photometry in one case and Sloan Digitized Sky Survey (SDSS) photometry (Jester et al. 2005) in the other two and obtained the V magnitude following the recipes in the above references. The flux ratio $\log(f_X/f_V)$ are listed in Table 1.

3. RESULTS

In the following we describe details of each object in the sample including related information in the literature.

3.1. ESO 352-41 ULX1

There is a spatially unresolved radio source at the ULX position, detected in RACS. However, no radio source is detected in VLASS above 4σ with an rms of 0.14 mJy at 3 GHz. The source was detected with ATCA on 2025 Dec 22 and 25, respectively, at both 5.5 GHz and 9 GHz. No optical counterpart can be seen in the DES image, with an upper limit of 23.1 mag on the r -band.

3.2. NGC 925 ULX1

An unresolved radio source in VLASS is detected at the ULX position. The ULX displays a high luminosity varying in the range of $(1 - 5) \times 10^{40}$ erg s $^{-1}$ with weak spectral variability (Pintore et al. 2018; Salvaggio et al. 2022). The spectrum of its infrared counterpart shows no continuum but is dominated by an [Fe II] $\lambda 16440$ emission line plus many other weaker emission lines, likely due to shocks harder than typical supernova remnants or X-ray illumination of surrounding materials (Heida et al. 2016). Lara-López et al. (2021) revealed a large (285 pc diameter) optical emission line nebula around the source with low metallicity, in agreement with the results reported in Heida et al. (2016).

3.3. NGC 1332 ULX2

This is the second brightest X-ray source in NGC 1332 and is outside the D25 isophotal diameter of the galaxy

Table 1. ULXs with radio counterparts in the RACS and/or VLASS surveys.

No.	Name	R.A.	Dec.	r_{err}	D	CatX	L_{X}	V	$\log(f_{\text{X}}/f_V)$	Nature
		(J2000)	(J2000)	($''$)	(Mpc)	$(10^{40} \text{ erg s}^{-1})$				
		(1)	(2)	(3)	(4)	(5)	(6)	(7)	(8)	(9)
1	ESO 352-41 ULX1	01 19 07.1	-34 07 05	4.0	78.4	4XMM	0.1	> 23.2	> -0.50	III
2	NGC 925 ULX1	02 27 27.5	+33 34 42	0.8	8.7	4XMM	4.5	20.3	1.90	III
3	NGC 1332 ULX2	03 26 14.8	-21 21 26	1.1	24.5	CSC2	0.4	21.6	0.75	I
4	PGC 146838 ULX1	05 01 07.9	-38 43 21	2.8	226.7	4XMM	32.0	19.5	-0.42	III
5	NGC 2207 ULX3	06 16 15.8	-21 22 03	1.2	36.4	CSC2	3.7	18.2	-0.25	II
6	NGC 2903 ULX3	09 32 09.8	+21 31 06	8.6	9.3	2SXPS	0.3	16.6	-0.85	II
7	NGC 3190 ULX1	10 18 04.3	+21 49 31	1.1	22.2	CSC2	0.1	24.3	1.32	I
8	ESO 171-5 ULX1	12 01 32.9	-53 21 36	9.3	59.9	2SXPS	7.7	16.7	-0.99	III
9	NGC 5018 ULX6	13 13 06.4	-19 31 14	2.2	34.0	4XMM	0.2	> 21.6	> -0.10	III
10	NGC 5457 ULX4	14 02 28.2	+54 16 26	1.0	7.0	4XMM	0.3	15.7	-0.89	II
11	NGC 5457 XMM88	14 03 53.9	+54 15 58	5.7	7.0	2SXPS	0.2	21.5	1.18	III
12	ESO 514-3 ULX1	15 18 37.1	-24 07 18	1.3	43.9	4XMM	2.5	> 21.0	> 0.51	I
13	NGC 5985 ULX1	15 39 39.8	+59 19 52	1.5	52.7	4XMM	8.7	21.1	0.93	III
14	NGC 6027 ULX1	15 59 10.3	+20 46 19	1.1	67.6	CSC2	0.2	20.8	-0.71	III
15	IC 4587 ULX1	15 59 49.5	+25 56 32	9.7	200.8	2SXPS	63.0	22.7	1.30	III
16	UGC 10143 ULX1	16 02 18.2	+15 59 12	1.5	140.6	CSC2	1.5	20.6	-0.64	III
17	NGC 6926 ULX1	20 33 05.9	-02 02 09	3.8	88.0	4XMM	2.6	> 19.2	> -0.80	II
18	NGC 6946 ULX1	20 35 00.7	+60 11 30	0.5	7.7	4XMM	2.1	19.7	1.41	III
19	PGC 90367 ULX1	20 37 17.2	+25 31 42	1.2	153.2	CSC2	1.5	> 18.6	> -1.60	II
20	NGC 7059 ULX1	21 27 29.2	-60 01 02	6.9	31.9	2SXPS	31.6	18.1	0.77	III
21	NGC 7648 ULX1	23 23 53.2	+09 39 59	1.3	52.2	CSC2	0.5	> 17.2	> -1.66	III

NOTE— Column (1): object number. Column (2): host galaxy and ULX name. Column (3): right ascension. Column (4): declination. Column (5): 3σ position error of a ULX quoted from [Walton et al. \(2022\)](#). Column (6): distance to the host galaxy adopted from [Walton et al. \(2022\)](#). Column (7): original X-ray catalog from which the position error is quoted. Column (8): peak X-ray luminosity in the unit of $10^{40} \text{ erg s}^{-1}$. Column (9): V -band magnitude translated from the photometry in PanSTARRS, DES-DR2, Gaia, or SDSS. Column (10): X-ray to optical flux ratio. Column (11): possible physical nature of the radio emissions: (I) background quasars, (II) star forming regions, or (III) accreting compact objects in the host galaxy.

([Humphrey & Buote 2004](#)). The radio images show a double lobed structure but no compact radio core is detected at the ULX position. ATCA observations confirmed the results. A point-like optical object at the ULX position can be seen in the DES image.

3.4. PGC 146838 ULX1

The RACS image shows an elongated structure with the ULX near the center. This structure is obviously attached to the host galaxy, and resolved into two parts in the VLASS image, one around the host galaxy and the other rooted at the ULX position. Interestingly, ATCA observations identified a point-like radio core at the ULX position with a flat spectrum ($\alpha \approx 0$); the VLASS image at the ULX position also shows an enhanced flux. A point-like optical counterpart is seen in the DES image.

3.5. NGC 2207 ULX3

This is source 28 in [Mineo et al. \(2013\)](#), source 3 in [Mineo et al. \(2014\)](#) and NGC 2207-1 in [Smith et al. \(2014\)](#), spatially coincident with a starburst region called *feature i* ([Elmegreen et al. 2000](#)). The authors also pointed out that the X-ray

source is extended and has a soft spectrum, suggesting that both the X-ray and radio emission could be due to starburst activity. However, [Mineo et al. \(2014\)](#) reported distinct X-ray fluxes measured from the source with four Chandra observations, varying in the range of $(0.8-6) \times 10^{-14} \text{ erg cm}^{-2} \text{ s}^{-1}$, suggesting that there could be a ULX embedded in an extended component.

3.6. NGC 2903 ULX3

It is the third most luminous X-ray source in NGC 2903 ([Pérez-Ramírez et al. 2010](#)). The ULX is spatially coincident with an extended H II region (source 36 with a radius of $6.4''$ in [Popping et al. 2010](#)). The radio emission is extended seen in the VLASS image. The VLASS radio contour seems to match the optical morphology in the PanSTARRS image.

3.7. NGC 3190 ULX1

A bright radio core plus two lobes are clearly detected with both RACS and VLASS. A faint optical counterpart is seen in the PanSTARRS image.

3.8. ESO 171-5 ULX1

Table 2. Radio peak flux density and spectral index.

Name	RACS		VLASS	ATCA		α	Remark
	0.9 GHz	1.4 GHz		3 GHz	5.5 GHz		
	(mJy)	(mJy)		(mJy)	(mJy)		
ESO 352-41 ULX1	1.4 ± 0.2	0.78 ± 0.15		0.121 ± 0.012	0.103 ± 0.013	-1.24 ± 0.08	
NGC 925 ULX1	2.2 ± 0.4	1.6 ± 0.3	0.60 ± 0.13			-1.1 ± 0.2	
NGC 1332 ULX2							lobes
PGC 146838 ULX1			0.96 ± 0.13	0.86 ± 0.04	0.864 ± 0.016	-0.03 ± 0.08	
NGC 2207 ULX3	25.0 ± 0.8	7.7 ± 0.7	2.66 ± 0.13	2.09 ± 0.04	1.029 ± 0.016	-1.260 ± 0.016	extended
NGC 2903 ULX3	12.2 ± 0.4	5.9 ± 0.9	1.03 ± 0.16			-2.00 ± 0.12	extended
NGC 3190 ULX1		1.2 ± 0.2	1.48 ± 0.14			0.3	core+lobes
ESO 171-5 ULX1	1.1 ± 0.2	0.82 ± 0.15		0.23 ± 0.05	0.150 ± 0.009	-0.88 ± 0.07	
NGC 5018 ULX6	1.2 ± 0.3	2.18 ± 0.16	2.1 ± 0.2	4.38 ± 0.03	6.21 ± 0.06	0.70 ± 0.02	
NGC 5457 ULX4			0.75 ± 0.11				extended
NGC 5457 XMM88			1.47 ± 0.11				
ESO 514-3 ULX1				0.34 ± 0.04	0.40 ± 0.03	0.3	core+lobes
NGC 5985 ULX1			0.60 ± 0.13				
NGC 6027 ULX1	10.3 ± 0.5	7.3 ± 0.2	5.07 ± 0.12			-0.52 ± 0.04	
IC 4587 ULX1	152.4 ± 0.3	107.2 ± 0.2	64.35 ± 0.14			-0.702 ± 0.002	
UGC 10143 ULX1	8.5 ± 0.5	6.1 ± 0.2	2.9 ± 0.2			-0.88 ± 0.07	
NGC 6926 ULX1			1.14 ± 0.17				extended
NGC 6946 ULX1			0.76 ± 0.18			-0.5†	
PGC 90367 ULX1			1.19 ± 0.14				extended
NGC 7059 ULX1	2.6 ± 0.2	1.8 ± 0.2		1.335 ± 0.012	0.698 ± 0.018	-0.61 ± 0.02	
NGC 7648 ULX1			0.57 ± 0.14				

NOTE—The error of flux is the noise rms and the error of α is at the 1σ level. Extended sources indicate that the integrated flux density is higher than the peak flux density by a factor of 2 or more.

† Quoted from Lacey et al. (1997).

The ULX has an unresolved radio counterpart in RACS. Within the X-ray position uncertainty (3σ radius $9''.3$), there is a GAIA source with a parallax distance of $2.2^{+0.4}_{-0.2}$ kpc (Bailer-Jones et al. 2021). The color and magnitude suggest that it is G-type main sequence star. Given the GAIA source density around the ULX and the X-ray position error, a chance coincidence with such a bright GAIA source in the field is about 0.1 and thus cannot be ruled out. Therefore, a more precise X-ray position is needed to confirm or reject the association.

3.9. NGC 5018 ULX6

The ULX shows an extremely hard X-ray spectrum with an optical counterpart identified in HST images with a magnitude of about 24 in F555W and F814W (see source 6 in Ghosh et al. 2005). With the HST magnitudes, we derived an X-ray to optical flux ratio of 0.9. Ghosh et al. (2005) reported the detection of a radio source at the ULX position, with a flux of 2.1 mJy at 1.4 GHz and an inverted spectrum ($\alpha \approx 0.2$), consist with the survey results in this work. They argued that it is a compact core of a background radio galaxy. Here our ATCA observations detected significant variation in the radio band.

3.10. NGC 5457 ULX4

The ULX is spatially coincident with NGC 5447 (Gordon et al. 2008), an H II region in M101 (= NGC 5457). The ULX is cataloged as source 4 in Jenkins et al. (2004), source 20 in Jenkins et al. (2005), X17 in Liu & Bregman (2005), XMM4 in Winter et al. (2006), and C21 in Berghea et al. (2008), and could be an X-ray binary embedded in the H II region. The VLASS image shows a small degree of extension compared with the beam pattern. Gajović et al. (2025) reported the radio emission from this H II region. The spectrum is a power-law with a slope $\alpha = -0.34$, without spectral flattening (absorption) down to 54 MHz, suggesting that the radio emission may arise from unresolved, separate small H II regions. We note that the ULX has displayed both short and long-term variability (Jenkins et al. 2005) and significant emission above 2 keV (Winter et al. 2006), indicating that it is an X-ray binary instead of emission from the hot gas.

3.11. NGC 5457 XMM88

The ULX is located at the outskirt of M101 (= NGC 5457) on the sky plane. The source is labeled as source 88 in Jenkins et al. (2005) from an XMM-Newton observation, during which the X-ray luminosity is only 1.3×10^{38} erg s $^{-1}$. In the

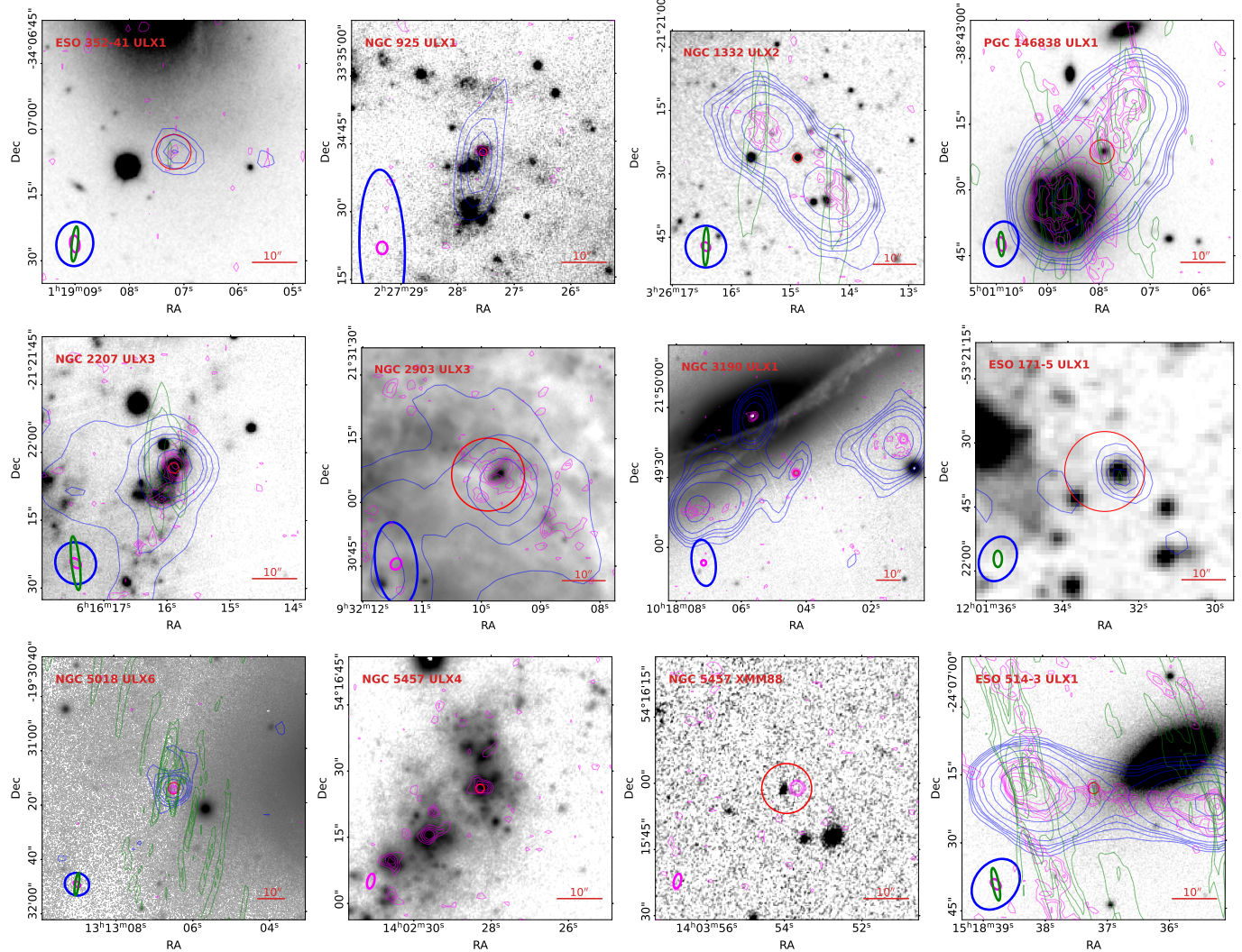


Figure 1. Radio contours around the ULX position on top of optical images. The red circle indicates the ULX position with a 3σ error radius. The contours are 2, 3, 4, 5, 8, 16, 32, and 64 times the rms noise level for RACS (blue) and VLASS (magenta), and 8, 16, 32, 64 and 128 times the rms for ATCA (green). The beam sizes are shown at the bottom left corner. The scale bar has a length of $10''$.

Chandra source catalog (Evans et al. 2010), the source flux is 2.85×10^{-14} erg cm $^{-2}$ s $^{-1}$, corresponding to a luminosity of 1.3×10^{38} erg s $^{-1}$ at a distance of 7 Mpc. However, the source was caught as a ULX with a Swift observation on 2011 December 6 at a luminosity of 2×10^{39} erg s $^{-1}$. The Swift detection has a 3σ position uncertainty of $5''.7$, consistent with the Chandra and XMM-Newton positions. If the X-ray emission detected from the three telescopes are due to the same source, then the Chandra position indicates that the X-ray position does not match the optical source in the PanSTARRS image. The radio source is a point-like object in the VLASS image, spatially coincident with the Chandra position.

3.12. ESO 514-3 ULX1

ESO 514-3 is a member of the NGC 5903 group. It has been reported by O'Sullivan et al. (2018) that the X-ray source is associated with a compact radio core plus a pair

of radio lobes, based on which the authors argued that it is a background AGN. They reported a core radio flux of about 1 mJy at 4.8 GHz, which is almost 2-3 times higher than our ATCA measurement. We note that the total radio flux densities including the core and the two lobes are consistent between the two works, suggesting that there may be temporal variability in the core radio emission. The optical counterpart is not visible in the PanSTARRS image, with an upper limit estimated to be $V = 21.0$, suggesting that $\log(f_X/f_V) > 0.5$.

3.13. NGC 5985 ULX1

The ULX appears at a sky position between two spiral arms, spatially coincident with an unresolved radio source in the VLASS image.

3.14. NGC 6027 ULX1

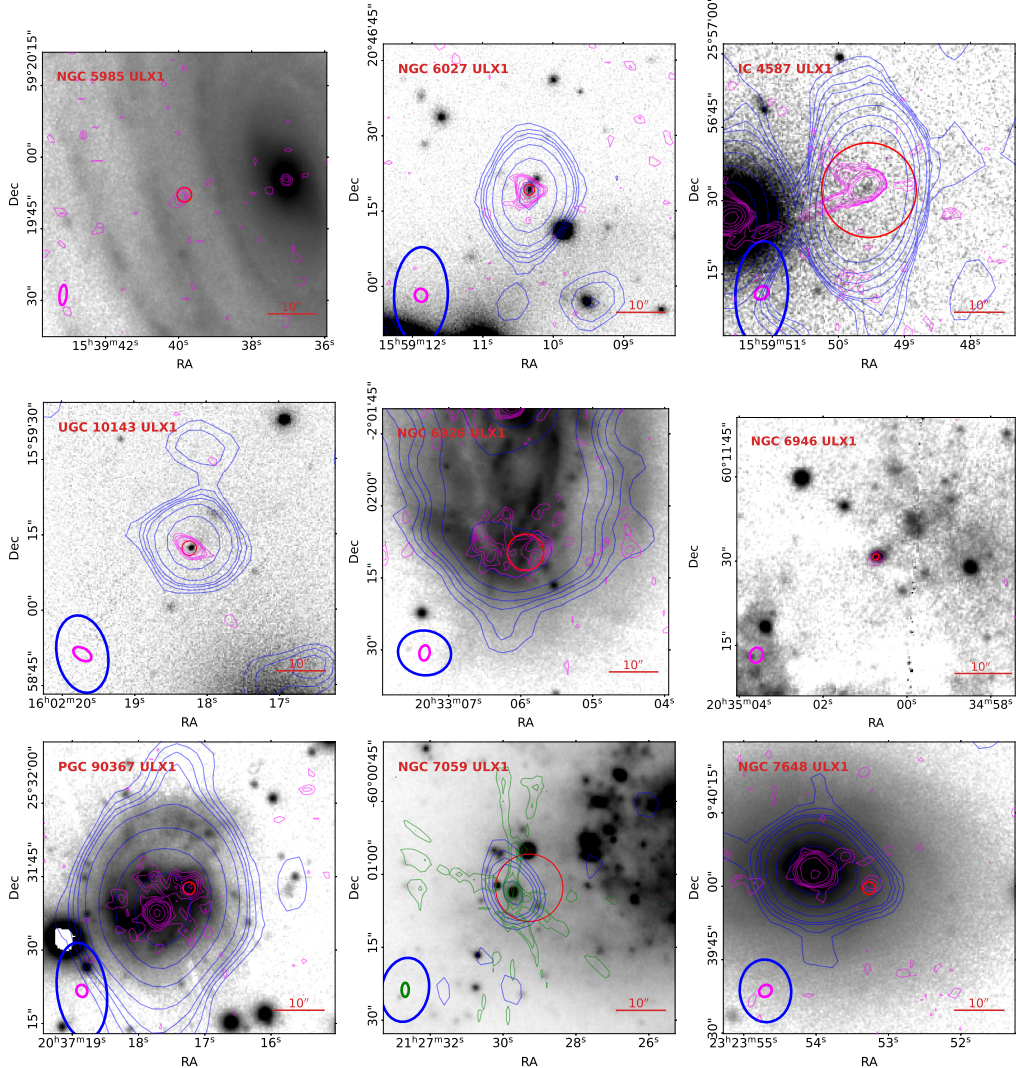
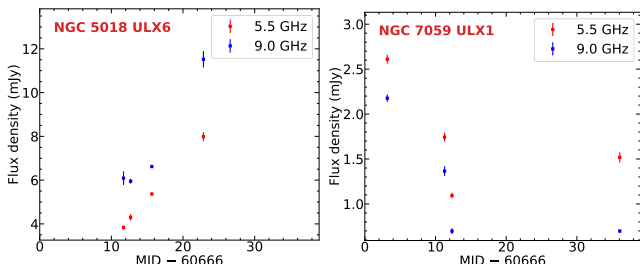


Figure 1. Continued.

Figure 2. ATCA radio lightcurves of NGC 5018 ULX6 and NGC 7059 ULX1 with 1σ error bars.

NGC 6027 is a member of the Seyfert's Sextet (HCG 79), and the X-ray source is spatially coincident with one of a pair, apparently interacting galaxies (Tamburri et al. 2012). With HST imaging, Palma et al. (2002) suspected that this object was a background spiral galaxy but no redshift measurement is available.

3.15. IC 4587 ULX1

The X-ray source is near a reddish optical object around the elliptical galaxy IC 4587. The radio source is included in the VLBA calibrator survey (Petrov 2021), who obtained a jet orientation (source elongation) of $145^\circ \pm 5^\circ$ by directly analyzing the calibrated visibilities.

3.16. UGC 10143 ULX1

The X-ray source appears near the elliptical radio galaxy UGC 10143 and has an optical counterpart. The radio source in both VLASS and RACS is unresolved.

3.17. NGC 6926 ULX1

The X-ray source is around the southern spiral arm of the Seyfert 2 Galaxy NGC 6926. The radio emission is extended as seen in VLASS, matching a star forming region in optical.

3.18. NGC 6946 ULX1

This is a well studied ULX in NGC 6946, embedded in an optical and radio nebula MF16 (van Dyk et al. 1994; Matonick & Fesen 1997; Lacey et al. 1997; Beuchert et al. 2024). The radio flux density measured with VLASS is consistent with that reported previously with VLA observations (source 85 in Lacey et al. 1997), with which the spectral index was measured as $\alpha = -0.5 \pm 0.1$. The radio emission is spatially resolved with VLA observations (van Dyk et al. 1994; Beuchert et al. 2024).

3.19. PGC 90367 ULX1

The X-ray source is around the spiral arm of PGC 90367. The radio emission in the VLASS image appears to be extended, with enhancement at the ULX position.

3.20. NGC 7059 ULX1

NGC 7059 is a spiral galaxy and unique for its association with a Fermi gamma-ray source 4FGL J2127.6–5959 (Abdullahi et al. 2020). The radio source has a point-like optical counterpart in the DES image. Therefore, it is likely that the radio, X-ray and gamma-ray emission is due to a background blazar. The ATCA observations detect significant variation in the radio band.

3.21. NGC 7648 ULX1

The ULX appears on the S0 galaxy NGC 7648 with ongoing star formation (Rose et al. 2001). Due to the brightness of the galaxy emission, no obvious optical counterpart can be identified in the PanSTARRS image. We note that the radio source associated with the ULX is not on the radial spokes of the nearby AGN.

4. DISCUSSION

Here we discuss their possible physical nature in three categories depending on the radio morphology and multiwavelength properties. This suggests that this sample has a diverse population.

4.1. Double lobed structures and background quasars

There are three objects where a double lobed radio structure is revealed around the ULX. They are NGC 1332 ULX2, NGC 3190 ULX1, and ESO 514-3 ULX1. Among them, NGC 3190 ULX1 and ESO 514-3 ULX1 also show a radio core associated with the ULX position. Multiband radio data suggest that they have a flat spectrum, reminiscent of a compact radio jet. A naive speculation is that these are not ULXs, but background quasars masqueraded as ULXs as they appear along the line of sight of a nearby galaxy. Based on ground-based optical survey images, NGC 1332 ULX2 and NGC 3190 ULX1 show a point-like optical counterpart, allowing us to estimate the X-ray-to-optical flux ratio $\log(f_X/f_V) = 0.75$ and 1.32, respectively. The ratios are consistent with those of AGNs or BL Lac objects (Maccacaro et al. 1988). For ESO 514-3, its X-ray-to-optical flux ratio (> 0.5), as well as the possible core radio flux variation, is consistent with the properties of an AGN or blazar. Following Landt et al. (2006), we calculated $L_{\text{core}}/L_{1\text{keV}}$ and

$L_{\text{core}}/L_{\text{lobe}}$, where L_{core} and L_{lobe} are the core and lobe luminosity densities at 1.4 GHz, respectively, and $L_{1\text{keV}}$ is the X-ray luminosity density at 1 keV, and found that the three sources all populate in the lobe-dominated regime and follow the correlation found for radio quasars.

Assuming that they follow the fundamental plane of accreting black holes, we may estimate the black hole mass using the relation in Merloni et al. (2003). The flux density at 5 GHz is estimated from the best-fit radio power-law spectrum. The inferred black hole mass is $5 \times 10^7 M_{\odot}$ for NGC 3190 ULX1 and $4 \times 10^6 M_{\odot}$ for ESO 514-3 ULX1, again consistent with the scenario that they are background quasars. To firmly determine their nature, a redshift measurement is needed.

Assuming that the three objects are background quasars, it sets a lower limit of the contamination ($3/21 \approx 14\%$) to the ULX catalog (Walton et al. 2022), consistent with their estimate of about 20%. However, one should be cautious as we have selected ULXs with radio emission, and the fraction of quasars with detectable radio emission is in general much higher than that of ULXs. An unbiased estimate can be obtained only if this factor can be corrected.

4.2. Radio emission due to star formation

The radio counterparts of five ULXs appear to be spatially extended, including NGC 2207 ULX3, NGC 2903 ULX3, NGC 5457 ULX4, NGC 6926 ULX1, and PGC 90367 ULX1, whose integrated flux densities are 5.8, 7.9, 1.5, 12.0, and 2.3 mJy, respectively, in the same order at 3 GHz measured with VLASS, which has a beam size smaller than RACS. They share a common property that the ULX resides in a star forming (H II) region seen in optical. Radio emission from H II regions is composed of two components, thermal free-free emission which generally has a flat spectrum and non-thermal synchrotron radiation which has a negative slope (typically $\alpha = -0.8$; Condon 1992; Murphy et al. 2011).

For two of them, the star formation rate of the corresponding H II region can be found in the literature, $1.6 M_{\odot} \text{ yr}^{-1}$ for NGC 2207 ULX3 (Elmegreen et al. 2016, 2017) and $0.126 M_{\odot} \text{ yr}^{-1}$ for NGC 2903 ULX3 (Popping et al. 2010). Given Eq. (17) in Murphy et al. (2011) and the measured spectral index, the thermal plus non-thermal radio flux density due to star formation is expected to be 5.5 and 4.1 mJy at 3 GHz, suggesting that most or part of the observed radio emission could be due to star forming activities. Their spectral indices are generally consistent with that of synchrotron radiation found in star forming regions (Tabatabaei et al. 2017; Galvin et al. 2018), although $\alpha \approx -2$ seen in NGC 2903 ULX3 is steeper than typical. Future high resolution radio observations are needed to investigate the nature of these sources. The X-ray emission with such a high luminosity is most likely coming from accreting compact objects in the H II region. Future long-term monitoring is needed to distinguish whether there is a single ULX (likely the cases of NGC 2207 ULX3 and NGC 5457 ULX4) or multiple X-ray binaries (no variability is expected with a total number of

~10–100 standard X-ray binaries to account for the observed luminosity).

4.3. Candidates for accreting compact objects in the host galaxy

For the rest thirteen objects with a compact radio counterpart, eight of them (ESO 352-41 ULX1, NGC 925 ULX1, ESO 171-5 ULX1, NGC 6027 ULX1, IC 4587 ULX1, UGC 10143 ULX1, NGC 6946 ULX1 and NGC 7059 ULX1) show a steep spectrum ($\alpha \leq -0.5$), two of them (PGC 146838 ULX1 and NGC 5018 ULX6) display a flat or inverted spectrum ($\alpha \gtrsim 0$), and the other three sources do not have multiple frequency bands available for a slope measurement.

Assuming that they reside in the apparent host galaxy, we discuss the nature of radio emission in two possible scenarios: jet/wind powered nebula due to supercritical accretion (SS 433/W50 like objects), or compact radio jets from accreting black holes. Of course, it is also possible that the radio emission is unrelated to the X-ray source or accretion mechanism, but due to a compact star forming region as discussed above; this can be identified with future optical spectroscopy.

Radio emission from shock-ionized nebulae due to jets/winds is mainly optically thin synchrotron radiation with a steep spectrum. If SS 433 at a distance of 5 kpc (Su et al. 2018) were observed in a nearby galaxy, it may appear as a small-scale or compact radio source, e.g., with an extension of 3''.6 at 10 Mpc or 0''.36 at 100 Mpc, and have a relatively weak flux density, e.g., 18 μ Jy at 10 Mpc or 0.18 μ Jy at 100 Mpc. Of course, the size and flux depend on the jet/wind mechanical power. In our sample, NGC 6946 ULX1 is a well studied, prototypical ULX and could be an interesting analog. However, its surrounding optical nebula MF16 is mainly powered by photoionization although shock-ionization is also important (Abolmasov et al. 2007). Thus, here we estimate the contribution of free-free emission to the observed radio flux based on the observed $H\beta$ luminosity. Adopting the relation between the $H\beta$ and radio emissivity of star forming regions (Caplan & Deharveng 1986), we estimate that the radio flux density due to free-free emission is 0.08–0.12 mJy at 3 GHz given an $H\beta$ luminosity of 1.8×10^{38} erg s $^{-1}$ (translated to a distance of 7.7 Mpc assumed in this work) and a temperature in the range of $(0.9–2) \times 10^4$ K (Abolmasov et al. 2008). Compared with the measurement of 0.76 mJy at 3 GHz, this suggests that only a small fraction of the radio emission can be attributed to free-free emission. It is worth noting that NGC 925 ULX1 is associated with an optical nebula (see § 3.2), further strengthening its analogy with NGC 6946 ULX1. Therefore, the sources with a steep radio spectrum are good candidates for SS 433/W50 like objects in external galaxies and deserve in-depth multiwavelength studies in the future.

Those with a flat or inverted spectrum resemble radio emission from a self-absorbed compact jet (Blandford & Königl 1979). Accreting black holes with radio emission in such a state are supposed to follow the fundamental plane of black hole activity (Falcke et al. 2004; Corbel et al. 2013). Following Merloni et al. (2003), we estimated a black hole mass

as $1.3 \times 10^8 M_\odot$ and $4.0 \times 10^8 M_\odot$, respectively, for PGC 146838 ULX1 ($\alpha = -0.03 \pm 0.08$) and NGC 5018 ULX6 ($\alpha = 0.70 \pm 0.02$). Thus, they are all typical supermassive black holes in this scenario. We note that the X-ray luminosities listed in Table 1 are peak luminosities rather than the values measured simultaneously with the radio and would lead to an underestimate of black hole masses to some extent. Black holes of such high masses are not expected to appear at an off-nuclear position over the cosmological timescale, and would have spiraled into the center of galaxy due to dynamical friction (Tremaine et al. 1975). Thus, finding an off-nuclear supermassive black hole is of great interest and may shed light on the evolution history of the host galaxy, e.g., they could be tidally stripped nuclei residing in a star cluster (Seth et al. 2014). We point out that these two objects as well as other objects discussed in this subsection all have an X-ray-to-optical flux ratio consistent with the range of AGNs (Maccacaro et al. 1988). Optical spectroscopy can test if they are indeed AGNs via emission line properties (e.g., the presence of broad lines) and the BPT (Baldwin–Phillips–Terlevich) diagram (Baldwin et al. 1981; Kewley et al. 2019; Law et al. 2021).

For the eight objects with a steep spectrum, we tend not to estimate their black hole mass using the fundamental plane. First, their radio emission may have an origin different from compact radio jets as discussed above, like the cases of NGC 925 ULX1 and NGC 6946 ULX1 where the radio emission is likely due to optically thin synchrotron radiation from the nebula. Second, these sources may be similar to compact steep-spectrum or peaked-spectrum radio sources (O’Dea & Saikia 2021), for which the fundamental plane is found to have a different relation (Fan & Bai 2016). We found that the inferred black hole masses of our sources using the relation in Fan & Bai (2016) are 4–6 orders of magnitude lower than those using the relation in Merloni et al. (2003). This is probably because the sample in Fan & Bai (2016) have an X-ray luminosity mostly higher than 10^{42} erg s $^{-1}$, and the application of their relation is a significant extrapolation in our cases.

We note that both NGC 5018 ULX6 ($\alpha = 0.70 \pm 0.02$) and NGC 7059 ULX1 ($\alpha = -0.61 \pm 0.02$) displayed significant radio variability on a timescale as short as one day. This suggests that the radio emission cannot arise from a large structure, but constrained in a region smaller than 10^{15} cm.

We also compared our sources with Fanaroff–Riley (FR) type 0 and type I radio galaxies in the plane of X-ray luminosity vs. radio luminosity (Torresi et al. 2018). There is only one object, IC 4587 ULX-1, well consistent with the FR0/FRI distribution in that plane. All other objects display a radio luminosity generally below the luminosity range of the sample in Torresi et al. (2018) and have an X-ray-to-radio luminosity ratio on average higher the FR0/FRI galaxies.

HLX-1 has an optical magnitude $V = 24.5$ (Soria et al. 2010a). Its X-ray peak luminosity is about 10^{42} erg s $^{-1}$ (Farrell et al. 2009), with an X-ray-to-optical flux ratio of about 3.2, higher than that of any sources in this work. If HLX-1 appears at a distance of 30 Mpc or closer, one ex-

pects $V \leq 22$, detectable with the optical surveys used in this work. Therefore, this work does not find any IMBH candidates typical of HLX-1 as we preferentially select radio-loud accretion systems. HLX-1 was found to display radio emission around $20 \mu\text{Jy}$ in its hard state (Cseh et al. 2015). This approaches the detection limit of the two surveys if the source is located within 30 Mpc. It is interesting to note that the mass of HLX-1 estimated from the fundamental plane is about $3 \times 10^6 M_\odot$ using the relation in Miller-Jones et al. (2012) or $7 \times 10^5 M_\odot$ using that in Merloni et al. (2003). These are both higher than the mass estimated from X-ray luminosities and temperatures (Servillat et al. 2011; Soria et al. 2017), typically on the order of $10^4 M_\odot$. Therefore, one should be cautious if the fundamental plane can be applied to these cases or if there is Doppler boosting in radio emission.

5. SUMMARY

In this work, we found 21 ULXs with a radio counterpart with RACS and/or VLASS surveys:

- three are associated double lobed radio structures and may be quasars;
- five are associated with extended radio structure, and also spatially coincident with star forming regions in optical; their radio emission may be attributed to star forming activities but their steep spectrum indicates caveats; two of them show X-ray variability; the X-ray emissions are likely from ULXs in star forming regions;

- thirteen are associated with an unresolved radio source:
 - eight have a steep radio spectrum, including one prototypical ULX (NGC 6946 ULX1), being good candidates for SS 433/W50 like objects;
 - two have a flat or inverted spectrum and could be black holes with a compact jet; they are supermassive black holes based on the fundamental plane;
 - significant radio variability on timescales as short as one day is detected in two sources (one has an inverted spectrum, and the other has a steep spectrum and is associated with gamma-ray emission);

- a redshift determination of these sources is of key importance.

We thank the anonymous referee for useful comments. HF acknowledges funding support from the National Natural Science Foundation of China under the grant 12025301, and the Strategic Priority Research Program of the Chinese Academy of Sciences.

REFERENCES

Abbott, T. M. C., Adamów, M., Aguena, M., et al. 2021, ApJS, 255, 20, doi: [10.3847/1538-4365/ac00b3](https://doi.org/10.3847/1538-4365/ac00b3)

Abdollahi, S., Acero, F., Ackermann, M., et al. 2020, ApJS, 247, 33, doi: [10.3847/1538-4365/ab6bcb](https://doi.org/10.3847/1538-4365/ab6bcb)

Abolmasov, P. 2008, in American Institute of Physics Conference Series, Vol. 1054, Cool Discs, Hot Flows: The Varying Faces of Accreting Compact Objects, ed. M. Axelsson (AIP), 33–38, doi: [10.1063/1.3002506](https://doi.org/10.1063/1.3002506)

Abolmasov, P., Fabrika, S., Sholukhova, O., & Afanasiev, V. 2007, Astrophysical Bulletin, 62, 36, doi: [10.1134/S199034130701004X](https://doi.org/10.1134/S199034130701004X)

Abolmasov, P., Fabrika, S., Sholukhova, O., & Kotani, T. 2008, arXiv e-prints, arXiv:0809.0409, doi: [10.48550/arXiv.0809.0409](https://doi.org/10.48550/arXiv.0809.0409)

Amato, R., Quintin, E., Tranin, H., et al. 2025, A&A, 701, A7, doi: [10.1051/0004-6361/202555122](https://doi.org/10.1051/0004-6361/202555122)

Bachetti, M., Harrison, F. A., Walton, D. J., et al. 2014, Nature, 514, 202, doi: [10.1038/nature13791](https://doi.org/10.1038/nature13791)

Bailer-Jones, C. A. L., Rybizki, J., Fouesneau, M., Demleitner, M., & Andrae, R. 2021, AJ, 161, 147, doi: [10.3847/1538-3881/abd806](https://doi.org/10.3847/1538-3881/abd806)

Baldwin, J. A., Phillips, M. M., & Terlevich, R. 1981, PASP, 93, 5, doi: [10.1086/130766](https://doi.org/10.1086/130766)

Barrows, R. S., Mezcua, M., & Comerford, J. M. 2019, ApJ, 882, 181, doi: [10.3847/1538-4357/ab338a](https://doi.org/10.3847/1538-4357/ab338a)

Berghea, C. T., Johnson, M. C., Secrest, N. J., et al. 2020, ApJ, 896, 117, doi: [10.3847/1538-4357/ab9108](https://doi.org/10.3847/1538-4357/ab9108)

Berghea, C. T., Weaver, K. A., Colbert, E. J. M., & Roberts, T. P. 2008, ApJ, 687, 471, doi: [10.1086/591722](https://doi.org/10.1086/591722)

Beuchert, T., Middleton, M. J., Soria, R., et al. 2024, MNRAS, 534, 645, doi: [10.1093/mnras/stae1975](https://doi.org/10.1093/mnras/stae1975)

Blandford, R. D., & Königl, A. 1979, ApJ, 232, 34, doi: [10.1086/157262](https://doi.org/10.1086/157262)

Caplan, J., & Deharveng, L. 1986, A&A, 155, 297

Chambers, K. C., Magnier, E. A., Metcalfe, N., et al. 2016, arXiv e-prints, arXiv:1612.05560, doi: [10.48550/arXiv.1612.05560](https://doi.org/10.48550/arXiv.1612.05560)

Colbert, E. J. M., & Mushotzky, R. F. 1999, ApJ, 519, 89, doi: [10.1086/307356](https://doi.org/10.1086/307356)

Condon, J. J. 1992, ARA&A, 30, 575, doi: [10.1146/annurev.aa.30.090192.003043](https://doi.org/10.1146/annurev.aa.30.090192.003043)

Corbel, S., Coriat, M., Brocksopp, C., et al. 2013, MNRAS, 428, 2500, doi: [10.1093/mnras/sts215](https://doi.org/10.1093/mnras/sts215)

Cseh, D., Corbel, S., Kaaret, P., et al. 2012, *ApJ*, 749, 17, doi: [10.1088/0004-637X/749/1/17](https://doi.org/10.1088/0004-637X/749/1/17)

Cseh, D., Webb, N. A., Godet, O., et al. 2015, *MNRAS*, 446, 3268, doi: [10.1093/mnras/stu2363](https://doi.org/10.1093/mnras/stu2363)

Dubner, G. M., Holdaway, M., Goss, W. M., & Mirabel, I. F. 1998, *AJ*, 116, 1842, doi: [10.1086/300537](https://doi.org/10.1086/300537)

Duchesne, S. W., Thomson, A. J. M., Pritchard, J., et al. 2023, *PASA*, 40, e034, doi: [10.1017/pasa.2023.31](https://doi.org/10.1017/pasa.2023.31)

Duchesne, S. W., Grundy, J. A., Heald, G. H., et al. 2024, *PASA*, 41, e003, doi: [10.1017/pasa.2023.60](https://doi.org/10.1017/pasa.2023.60)

Earnshaw, H. P., Roberts, T. P., Middleton, M. J., Walton, D. J., & Mateos, S. 2019, *MNRAS*, 483, 5554, doi: [10.1093/mnras/sty3403](https://doi.org/10.1093/mnras/sty3403)

Elmegreen, B. G., Kaufman, M., Bournaud, F., et al. 2016, *ApJ*, 823, 26, doi: [10.3847/0004-637X/823/1/26](https://doi.org/10.3847/0004-637X/823/1/26)

Elmegreen, B. G., Kaufman, M., Struck, C., et al. 2000, *AJ*, 120, 630, doi: [10.1086/301462](https://doi.org/10.1086/301462)

Elmegreen, D. M., Elmegreen, B. G., Kaufman, M., et al. 2017, *ApJ*, 841, 43, doi: [10.3847/1538-4357/aa6ba5](https://doi.org/10.3847/1538-4357/aa6ba5)

Evans, I. N., Primini, F. A., Glotfelty, K. J., et al. 2010, *ApJS*, 189, 37, doi: [10.1088/0067-0049/189/1/37](https://doi.org/10.1088/0067-0049/189/1/37)

Evans, I. N., Evans, J. D., Martínez-Galarza, J. R., et al. 2024, *ApJS*, 274, 22, doi: [10.3847/1538-4365/ad6319](https://doi.org/10.3847/1538-4365/ad6319)

Evans, P. A., Page, K. L., Osborne, J. P., et al. 2020, *ApJS*, 247, 54, doi: [10.3847/1538-4365/ab7db9](https://doi.org/10.3847/1538-4365/ab7db9)

Fabrika, S. 2004, *Astrophys. Space Phys. Res.*, 12, 1, doi: [10.48550/arXiv.astro-ph/0603390](https://doi.org/10.48550/arXiv.astro-ph/0603390)

Fabrika, S. N., Atapin, K. E., Vinokurov, A. S., & Sholukhova, O. N. 2021, *Astrophysical Bulletin*, 76, 6, doi: [10.1134/S1990341321010077](https://doi.org/10.1134/S1990341321010077)

Falcke, H., Körding, E., & Markoff, S. 2004, *A&A*, 414, 895, doi: [10.1051/0004-6361:20031683](https://doi.org/10.1051/0004-6361:20031683)

Fan, X.-L., & Bai, J.-M. 2016, *ApJ*, 818, 185, doi: [10.3847/0004-637X/818/2/185](https://doi.org/10.3847/0004-637X/818/2/185)

Farrell, S. A., Webb, N. A., Barret, D., Godet, O., & Rodrigues, J. M. 2009, *Nature*, 460, 73, doi: [10.1038/nature08083](https://doi.org/10.1038/nature08083)

Feng, H., & Kaaret, P. 2005, *ApJ*, 633, 1052, doi: [10.1086/491597](https://doi.org/10.1086/491597)

—. 2010, *ApJL*, 712, L169, doi: [10.1088/2041-8205/712/2/L169](https://doi.org/10.1088/2041-8205/712/2/L169)

Gaia Collaboration, Vallenari, A., Brown, A. G. A., et al. 2023, *A&A*, 674, A1, doi: [10.1051/0004-6361/202243940](https://doi.org/10.1051/0004-6361/202243940)

Gajović, L., Heesen, V., Brüggen, M., et al. 2025, *A&A*, 695, A41, doi: [10.1051/0004-6361/202453003](https://doi.org/10.1051/0004-6361/202453003)

Galvin, T. J., Seymour, N., Marvil, J., et al. 2018, *MNRAS*, 474, 779, doi: [10.1093/mnras/stx2613](https://doi.org/10.1093/mnras/stx2613)

Gao, Y., Wang, Q. D., Appleton, P. N., & Lucas, R. A. 2003, *ApJL*, 596, L171, doi: [10.1086/379598](https://doi.org/10.1086/379598)

Ghosh, K. K., Swartz, D. A., Tennant, A. F., Wu, K., & Saripalli, L. 2005, *ApJ*, 623, 815, doi: [10.1086/428939](https://doi.org/10.1086/428939)

Gordon, K. D., Engelbracht, C. W., Rieke, G. H., et al. 2008, *ApJ*, 682, 336, doi: [10.1086/589567](https://doi.org/10.1086/589567)

Gordon, Y. A., Boyce, M. M., O'Dea, C. P., et al. 2021, *ApJS*, 255, 30, doi: [10.3847/1538-4365/ac05c0](https://doi.org/10.3847/1538-4365/ac05c0)

Graham, A. W., Chilingarian, I., Nguyen, D. D., et al. 2025, *PASA*, 42, e068, doi: [10.1017/pasa.2025.10035](https://doi.org/10.1017/pasa.2025.10035)

Gúrpide, A., Parra, M., Godet, O., Contini, T., & Olive, J. F. 2022, *A&A*, 666, A100, doi: [10.1051/0004-6361/202142229](https://doi.org/10.1051/0004-6361/202142229)

Heida, M., Jonker, P. G., Torres, M. A. P., et al. 2016, *MNRAS*, 459, 771, doi: [10.1093/mnras/stw695](https://doi.org/10.1093/mnras/stw695)

Humphrey, P. J., & Buote, D. A. 2004, *ApJ*, 612, 848, doi: [10.1086/422743](https://doi.org/10.1086/422743)

Jenkins, L. P., Roberts, T. P., Warwick, R. S., Kilgard, R. E., & Ward, M. J. 2004, *MNRAS*, 349, 404, doi: [10.1111/j.1365-2966.2004.07546.x](https://doi.org/10.1111/j.1365-2966.2004.07546.x)

—. 2005, *MNRAS*, 357, 401, doi: [10.1111/j.1365-2966.2005.08645.x](https://doi.org/10.1111/j.1365-2966.2005.08645.x)

Jester, S., Schneider, D. P., Richards, G. T., et al. 2005, *AJ*, 130, 873, doi: [10.1086/432466](https://doi.org/10.1086/432466)

Jiang, Y.-F., Stone, J. M., & Davis, S. W. 2014, *ApJ*, 796, 106, doi: [10.1088/0004-637X/796/2/106](https://doi.org/10.1088/0004-637X/796/2/106)

Kaaret, P., Feng, H., & Roberts, T. P. 2017, *ARA&A*, 55, 303, doi: [10.1146/annurev-astro-091916-055259](https://doi.org/10.1146/annurev-astro-091916-055259)

Kewley, L. J., Nicholls, D. C., & Sutherland, R. S. 2019, *ARA&A*, 57, 511, doi: [10.1146/annurev-astro-081817-051832](https://doi.org/10.1146/annurev-astro-081817-051832)

King, A., Lasota, J.-P., & Middleton, M. 2023, *NewAR*, 96, 101672, doi: [10.1016/j.newar.2022.101672](https://doi.org/10.1016/j.newar.2022.101672)

Kitaki, T., Mineshige, S., Ohsuga, K., & Kawashima, T. 2021, *PASJ*, 73, 450, doi: [10.1093/pasj/psab011](https://doi.org/10.1093/pasj/psab011)

Kosec, P., Pinto, C., Fabian, A. C., & Walton, D. J. 2018, *MNRAS*, 473, 5680, doi: [10.1093/mnras/stx2695](https://doi.org/10.1093/mnras/stx2695)

Lacey, C., Duric, N., & Goss, W. M. 1997, *ApJS*, 109, 417, doi: [10.1086/312989](https://doi.org/10.1086/312989)

Lacy, M., Baum, S. A., Chandler, C. J., et al. 2020, *PASP*, 132, 035001, doi: [10.1088/1538-3873/ab63eb](https://doi.org/10.1088/1538-3873/ab63eb)

Landt, H., Perlman, E. S., & Padovani, P. 2006, *ApJ*, 637, 183, doi: [10.1086/498261](https://doi.org/10.1086/498261)

Lang, C. C., Kaaret, P., Corbel, S., & Mercer, A. 2007, *ApJ*, 666, 79, doi: [10.1086/519553](https://doi.org/10.1086/519553)

Lara-López, M. A., Zinchenko, I. A., Pilyugin, L. S., et al. 2021, *ApJ*, 906, 42, doi: [10.3847/1538-4357/abc892](https://doi.org/10.3847/1538-4357/abc892)

Law, D. R., Ji, X., Belfiore, F., et al. 2021, *ApJ*, 915, 35, doi: [10.3847/1538-4357/abfe0a](https://doi.org/10.3847/1538-4357/abfe0a)

Liu, J.-F., & Bregman, J. N. 2005, *ApJS*, 157, 59, doi: [10.1086/427170](https://doi.org/10.1086/427170)

Maccacaro, T., Gioia, I. M., Wolter, A., Zamorani, G., & Stocke, J. T. 1988, *ApJ*, 326, 680, doi: [10.1086/166127](https://doi.org/10.1086/166127)

MacKenzie, A. D. A., Roberts, T. P., & Walton, D. J. 2023, *Astronomische Nachrichten*, 344, e20230028, doi: [10.1002/asna.20230028](https://doi.org/10.1002/asna.20230028)

Magnier, E. A., Schlafly, E. F., Finkbeiner, D. P., et al. 2020, *ApJS*, 251, 6, doi: [10.3847/1538-4365/abb82a](https://doi.org/10.3847/1538-4365/abb82a)

Matonick, D. M., & Fesen, R. A. 1997, *ApJS*, 112, 49, doi: [10.1086/313034](https://doi.org/10.1086/313034)

McConnell, D., Hale, C. L., Lenc, E., et al. 2020, *PASA*, 37, e048, doi: [10.1017/pasa.2020.41](https://doi.org/10.1017/pasa.2020.41)

McLeod, A. F., Scaringi, S., Soria, R., et al. 2019, *MNRAS*, 485, 3476, doi: [10.1093/mnras/stz614](https://doi.org/10.1093/mnras/stz614)

McMullin, J. P., Waters, B., Schiebel, D., Young, W., & Golap, K. 2007, in *Astronomical Society of the Pacific Conference Series*, Vol. 376, *Astronomical Data Analysis Software and Systems XVI*, ed. R. A. Shaw, F. Hill, & D. J. Bell, 127

Meier, D. L. 1982, *ApJ*, 256, 681, doi: [10.1086/159942](https://doi.org/10.1086/159942)

Merloni, A., Heinz, S., & di Matteo, T. 2003, *MNRAS*, 345, 1057, doi: [10.1046/j.1365-2966.2003.07017.x](https://doi.org/10.1046/j.1365-2966.2003.07017.x)

Mezcua, M., Farrell, S. A., Gladstone, J. C., & Lobanov, A. P. 2013, *MNRAS*, 436, 1546, doi: [10.1093/mnras/stt1674](https://doi.org/10.1093/mnras/stt1674)

Mezcua, M., & Lobanov, A. P. 2011, *Astronomische Nachrichten*, 332, 379, doi: [10.1002/asna.201011504](https://doi.org/10.1002/asna.201011504)

Miller, N. A., Mushotzky, R. F., & Neff, S. G. 2005, *ApJL*, 623, L109, doi: [10.1086/430112](https://doi.org/10.1086/430112)

Miller-Jones, J. C. A., Wrobel, J. M., Sivakoff, G. R., et al. 2012, *ApJL*, 755, L1, doi: [10.1088/2041-8205/755/1/L1](https://doi.org/10.1088/2041-8205/755/1/L1)

Mineo, S., Rappaport, S., Levine, A., et al. 2014, *ApJ*, 797, 91, doi: [10.1088/0004-637X/797/2/91](https://doi.org/10.1088/0004-637X/797/2/91)

Mineo, S., Rappaport, S., Steinhorn, B., et al. 2013, *ApJ*, 771, 133, doi: [10.1088/0004-637X/771/2/133](https://doi.org/10.1088/0004-637X/771/2/133)

Murphy, E. J., Condon, J. J., Schinnerer, E., et al. 2011, *ApJ*, 737, 67, doi: [10.1088/0004-637X/737/2/67](https://doi.org/10.1088/0004-637X/737/2/67)

O'Dea, C. P., & Saikia, D. J. 2021, *A&A Rv*, 29, 3, doi: [10.1007/s00159-021-00131-w](https://doi.org/10.1007/s00159-021-00131-w)

Ohsuga, K., & Mineshige, S. 2011, *ApJ*, 736, 2, doi: [10.1088/0004-637X/736/1/2](https://doi.org/10.1088/0004-637X/736/1/2)

O'Sullivan, E., Kolokythas, K., Kantharia, N. G., et al. 2018, *MNRAS*, 473, 5248, doi: [10.1093/mnras/stx2702](https://doi.org/10.1093/mnras/stx2702)

Pakull, M. W., & Mirioni, L. 2002, *arXiv e-prints*, astro, doi: [10.48550/arXiv.astro-ph/0202488](https://doi.org/10.48550/arXiv.astro-ph/0202488)

Pakull, M. W., & Mirioni, L. 2003, in *Revista Mexicana de Astronomia y Astrofisica Conference Series*, Vol. 15, *Revista Mexicana de Astronomia y Astrofisica Conference Series*, ed. J. Arthur & W. J. Henney, 197–199

Pakull, M. W., Soria, R., & Motch, C. 2010, *Nature*, 466, 209, doi: [10.1038/nature09168](https://doi.org/10.1038/nature09168)

Palma, C., Zonak, S. G., Hunsberger, S. D., et al. 2002, *AJ*, 124, 2425, doi: [10.1086/344160](https://doi.org/10.1086/344160)

Pannuti, T. G., Duric, N., Lacey, C. K., et al. 2002, *ApJ*, 565, 966, doi: [10.1086/337918](https://doi.org/10.1086/337918)

Pasham, D. R., Strohmayer, T. E., & Mushotzky, R. F. 2014, *Nature*, 513, 74, doi: [10.1038/nature13710](https://doi.org/10.1038/nature13710)

Pérez-Ramírez, D., Caballero-García, M. D., Ebrero, J., & Leon, S. 2010, *A&A*, 522, A53, doi: [10.1051/0004-6361/201015812](https://doi.org/10.1051/0004-6361/201015812)

Petrov, L. 2021, *AJ*, 161, 14, doi: [10.3847/1538-3881/abc4e1](https://doi.org/10.3847/1538-3881/abc4e1)

Petrov, L. Y., & Kovalev, Y. Y. 2025, *ApJS*, 276, 38, doi: [10.3847/1538-4365/ad8c36](https://doi.org/10.3847/1538-4365/ad8c36)

Pinto, C., Middleton, M. J., & Fabian, A. C. 2016, *Nature*, 533, 64, doi: [10.1038/nature17417](https://doi.org/10.1038/nature17417)

Pinto, C., & Walton, D. J. 2023, *arXiv e-prints*, arXiv:2302.00006, doi: [10.48550/arXiv.2302.00006](https://doi.org/10.48550/arXiv.2302.00006)

Pinto, C., Alston, W., Soria, R., et al. 2017, *MNRAS*, 468, 2865, doi: [10.1093/mnras/stx641](https://doi.org/10.1093/mnras/stx641)

Pinto, C., Soria, R., Walton, D. J., et al. 2021, *MNRAS*, 505, 5058, doi: [10.1093/mnras/stab1648](https://doi.org/10.1093/mnras/stab1648)

Pintore, F., Zampieri, L., Mereghetti, S., et al. 2018, *MNRAS*, 479, 4271, doi: [10.1093/mnras/sty1766](https://doi.org/10.1093/mnras/sty1766)

Popping, G., Pérez, I., & Zurita, A. 2010, *A&A*, 521, A8, doi: [10.1051/0004-6361/201014183](https://doi.org/10.1051/0004-6361/201014183)

Poutanen, J., Lipunova, G., Fabrika, S., Butkevich, A. G., & Abolmasov, P. 2007, *MNRAS*, 377, 1187, doi: [10.1111/j.1365-2966.2007.11668.x](https://doi.org/10.1111/j.1365-2966.2007.11668.x)

Ramsey, C. J., Williams, R. M., Gruendl, R. A., et al. 2006, *ApJ*, 641, 241, doi: [10.1086/499070](https://doi.org/10.1086/499070)

Rose, J. A., Gaba, A. E., Caldwell, N., & Chaboyer, B. 2001, *AJ*, 121, 793, doi: [10.1086/318754](https://doi.org/10.1086/318754)

Russell, D. M., Yang, Y. J., Gladstone, J. C., Wiersema, K., & Roberts, T. P. 2011, *Astronomische Nachrichten*, 332, 371, doi: [10.1002/asna.201011502](https://doi.org/10.1002/asna.201011502)

Salvaggio, C., Wolter, A., Pintore, F., et al. 2022, *MNRAS*, 512, 1814, doi: [10.1093/mnras/stac559](https://doi.org/10.1093/mnras/stac559)

Sánchez-Sutil, J. R., Muñoz-Arjonilla, A. J., Martí, J., et al. 2006, *A&A*, 452, 739, doi: [10.1051/0004-6361:20054688](https://doi.org/10.1051/0004-6361:20054688)

Servillat, M., Farrell, S. A., Lin, D., et al. 2011, *ApJ*, 743, 6, doi: [10.1088/0004-637X/743/1/6](https://doi.org/10.1088/0004-637X/743/1/6)

Seth, A. C., van den Bosch, R., Mieske, S., et al. 2014, *Nature*, 513, 398, doi: [10.1038/nature13762](https://doi.org/10.1038/nature13762)

Sądowski, A., & Narayan, R. 2016, *MNRAS*, 456, 3929, doi: [10.1093/mnras/stv2941](https://doi.org/10.1093/mnras/stv2941)

Smith, B. J., Soria, R., Struck, C., et al. 2014, *AJ*, 147, 60, doi: [10.1088/0004-6256/147/3/60](https://doi.org/10.1088/0004-6256/147/3/60)

Soria, R., Blair, W. P., Long, K. S., Russell, T. D., & Winkler, P. F. 2020, *ApJ*, 888, 103, doi: [10.3847/1538-4357/ab5b0c](https://doi.org/10.3847/1538-4357/ab5b0c)

Soria, R., Hau, G. K. T., Graham, A. W., et al. 2010a, *MNRAS*, 405, 870, doi: [10.1111/j.1365-2966.2010.16517.x](https://doi.org/10.1111/j.1365-2966.2010.16517.x)

Soria, R., Long, K. S., Blair, W. P., et al. 2014, *Science*, 343, 1330, doi: [10.1126/science.1248759](https://doi.org/10.1126/science.1248759)

Soria, R., Musaeva, A., Wu, K., et al. 2017, *MNRAS*, 469, 886, doi: [10.1093/mnras/stx888](https://doi.org/10.1093/mnras/stx888)

Soria, R., Pakull, M. W., Broderick, J. W., Corbel, S., & Motch, C. 2010b, *MNRAS*, 409, 541, doi: [10.1111/j.1365-2966.2010.17360.x](https://doi.org/10.1111/j.1365-2966.2010.17360.x)

Soria, R., Pakull, M. W., Motch, C., et al. 2021, *MNRAS*, 501, 1644, doi: [10.1093/mnras/staa3784](https://doi.org/10.1093/mnras/staa3784)

Su, Y., Zhou, X., Yang, J., et al. 2018, *ApJ*, 863, 103, doi: [10.3847/1538-4357/aad04e](https://doi.org/10.3847/1538-4357/aad04e)

Sutton, A. D., Roberts, T. P., Walton, D. J., Gladstone, J. C., & Scott, A. E. 2012, *MNRAS*, 423, 1154, doi: [10.1111/j.1365-2966.2012.20944.x](https://doi.org/10.1111/j.1365-2966.2012.20944.x)

Tabatabaei, F. S., Schinnerer, E., Krause, M., et al. 2017, *ApJ*, 836, 185, doi: [10.3847/1538-4357/836/2/185](https://doi.org/10.3847/1538-4357/836/2/185)

Tamburri, S., Trinchieri, G., Wolter, A., et al. 2012, *A&A*, 541, A28, doi: [10.1051/0004-6361/201118758](https://doi.org/10.1051/0004-6361/201118758)

Tao, L., Feng, H., Grisé, F., & Kaaret, P. 2011, *ApJ*, 737, 81, doi: [10.1088/0004-637X/737/2/81](https://doi.org/10.1088/0004-637X/737/2/81)

Torresi, E., Grandi, P., Capetti, A., Baldi, R. D., & Giovannini, G. 2018, *MNRAS*, 476, 5535, doi: [10.1093/mnras/sty520](https://doi.org/10.1093/mnras/sty520)

Tranin, H., Webb, N., Godet, O., & Quintin, E. 2024, *A&A*, 681, A16, doi: [10.1051/0004-6361/202244952](https://doi.org/10.1051/0004-6361/202244952)

Tremaine, S. D., Ostriker, J. P., & Spitzer, Jr., L. 1975, *ApJ*, 196, 407, doi: [10.1086/153422](https://doi.org/10.1086/153422)

Urquhart, R., Soria, R., Johnston, H. M., et al. 2018, *MNRAS*, 475, 3561, doi: [10.1093/mnras/sty014](https://doi.org/10.1093/mnras/sty014)

Urquhart, R., Soria, R., Pakull, M. W., et al. 2019, *MNRAS*, 482, 2389, doi: [10.1093/mnras/sty2771](https://doi.org/10.1093/mnras/sty2771)

van Dyk, S. D., Sramek, R. A., Weiler, K. W., Hyman, S. D., & Virden, R. E. 1994, *ApJL*, 425, L77, doi: [10.1086/187314](https://doi.org/10.1086/187314)

Walton, D. J., Mackenzie, A. D. A., Gully, H., et al. 2022, *MNRAS*, 509, 1587, doi: [10.1093/mnras/stab3001](https://doi.org/10.1093/mnras/stab3001)

Walton, D. J., Middleton, M. J., Pinto, C., et al. 2016, *ApJL*, 826, L26, doi: [10.3847/2041-8205/826/2/L26](https://doi.org/10.3847/2041-8205/826/2/L26)

Webb, N., Cseh, D., Lenc, E., et al. 2012, *Science*, 337, 554, doi: [10.1126/science.1222779](https://doi.org/10.1126/science.1222779)

Webb, N. A., Coriat, M., Traulsen, I., et al. 2020, *A&A*, 641, A136, doi: [10.1051/0004-6361/201937353](https://doi.org/10.1051/0004-6361/201937353)

Winter, L. M., Mushotzky, R. F., & Reynolds, C. S. 2006, *ApJ*, 649, 730, doi: [10.1086/506579](https://doi.org/10.1086/506579)

Zhou, C., Bian, F., Feng, H., & Huang, J. 2022, *ApJ*, 935, 38, doi: [10.3847/1538-4357/ac815f](https://doi.org/10.3847/1538-4357/ac815f)

Zhou, C., Feng, H., & Bian, F. 2023a, *ApJ*, 947, 52, doi: [10.3847/1538-4357/acc5eb](https://doi.org/10.3847/1538-4357/acc5eb)

—. 2023b, *ApJ*, 955, 61, doi: [10.3847/1538-4357/acf374](https://doi.org/10.3847/1538-4357/acf374)